View metadata, citation and similar papers at core.ac.uk
brought to you by CORE
provided by Digital.CSIC

Mon. Not. R. Astron. Soc. **000**, 1–?? (2010) Printed 28 September 2010 (MN LATEX style file v2.2)

New constraints on Parity Symmetry from a re-analysis of the WMAP-7 low resolution power spectra

A. Gruppuso [1,2⋆], F. Finelli [1,2], P. Natoli [3,4,5], F. Paci [6], P. Cabella [3]
A. De Rosa [1], N. Mandolesi [1]

[1] *INAF-IASF Bologna, Istituto di Astrofisica Spaziale e Fisica Cosmica di Bologna Istituto Nazionale di Astrofisica, via Gobetti 101, I-40129 Bologna, Italy*
[2] *INFN, Sezione di Bologna, Via Irnerio 46, I-40126 Bologna, Italy*
[3] *Dipartimento di Fisica, Università di Roma Tor Vergata, Via della Ricerca Scientifica 1, 00133 Roma, Italy*
[4] *INFN, Sezione di Roma Tor Vergata, Via della Ricerca Scientifica 1, 00133 Roma, Italy*
[5] *ASI Science Data Center, c/o ESRIN, via G. Galilei, I-00044 Frascati, Italy*
[6] *Instituto de Física de Cantabria (CSIC - Univ. de Cantabria), Avda. Los Castros s/n, 39005 Santander, Spain*

arXiv:1006.1979v2 [astro-ph.CO] 27 Sep 2010

28 September 2010

ABSTRACT

The Parity symmetry of the Cosmic Microwave Background (CMB) pattern as seen by WMAP 7 is tested *jointly in temperature and polarization* at large angular scale. A Quadratic Maximum Likelihood (QML) estimator is applied to the WMAP 7 year low resolution maps to compute all polarized CMB angular power spectra. The analysis is supported by 10000 realistic Monte-Carlo realizations. We confirm the previously reported Parity anomaly for TT in the range $\delta\ell = [2, 22]$ at $> 99.5\%$ C.L.. No anomalies have been detected in TT for a wider ℓ range (up to $\ell_{max} = 40$). No violations have been found for EE, TE and BB which we test here for the first time. The cross-spectra TB and EB are found to be consistent with zero. We also forecast PLANCK capabilities in probing Parity violations on low resolution maps.

Key words: cosmic microwave background - cosmology: theory - methods: numerical - methods: statistical - cosmology: observations

1 INTRODUCTION

The anisotropy pattern of the cosmic microwave background (CMB), measured by the Wilkinson Microwave Anisotropy Probe (WMAP), probes cosmology with unprecedented precision (see Larson et al. (2010); Komatsu et al. (2010) and references therein). WMAP data are largely consistent with the concordance Λ cold dark matter (ΛCDM) model, but there are some interesting deviations from it, in particular on the largest angular scales (Copi et al. 2010). See also (Bennett et al. 2010) for a critical point of view upon the subject.

A large number of papers dealing with these anomalies have been published in the last years. We list below those that are the most studied: a) lack of power on large angular scales. The angular correlation function is found to be uncorrelated (i.e., consistent with zero) for angles larger than 60°. In (Copi et al. 2007, 2009), it was shown that this event happens in only 0.03% of realizations of the concordance model. b) Hemispherical asymmetries. It is found that the power in temperature coming separately from the two hemispheres (defined by the ecliptic plane) is unlikely asymmetric (Eriksen et al. 2004; Hansen, Banday and Gorski 2004). It has been confirmed in the WMAP 3 year and 5 year release (Eriksen et al. 2007; Hansen et al. 2009; Hoftuft et al. 2009) and it is present in the COBE data as well, although with lower significance. The temperature power spectra of the opposing hemispheres are inconsistent at 3σ to 4σ depending on the range of multipoles considered. The asymmetry has been detected in low resolution maps (Eriksen et al. 2004), both in angular and multipoles space, but it extends to much smaller angular scales in the multipole range $\delta\ell = [2, 600]$ (Hansen et al. 2009). At large angular scales the hemispherical asymmetry has been tested for the first time in polarization maps in (Paci et al. 2010) making clear that this anomaly is evident only in intensity at WMAP sensitivity. c) Unlikely alignments of low multipoles. An unlikely (for a statistically isotropic random field) alignment of the quadrupole and the octupole is found in (Tegmark, de Oliveira-Costa and Hamilton 2003; Copi, Huterer and Starkman 2004; Schwarz et al. 2004; Weeks 2004; Land and Magueijo 2005a). Both quadrupole and octupole are shown to align with the CMB dipole (Copi et al. 2007). Other unlikely alignments are described

⋆ E-mail: gruppuso@iasfbo.inaf.it

in (Abramo et al. 2006; Wiaux et al. 2006; Vielva et al. 2007; Gruppuso and Gorski 2010) and a test for detecting foreground residuals in the alignement estimators is present in (Gruppuso and Burigana 2009). d) Non-Gaussianity. Vielva et al. (2004) detected a localized non-Gaussian behavior in the southern hemisphere (called Cold Spot) using a wavelet analysis technique (see also Cruz et al. (2005, 2009)). Large scales non-Gaussian analyses can be found in (Bernui and Reboucas 2010; Bernui, Reboucas and Teixeira 2010). See also Pietrobon et al. (2009) where the needlet formalism has been applied to the WMAP 5 year data, looking for evidence of non-Gaussianity in the bispectrum of the needlet amplitudes. e) Parity asymmetry. It has been suggested in (Land and Magueijo 2005b) that an estimator built upon the point parity symmetry might be used as a practical tool for detecting foregrounds. In particular these authors consider whether the observed low CMB quadrupole in temperature could more generally signal odd point-parity, i.e. suppression of even multipoles. However they claim that WMAP dataset never supports parity preference beyond the meagre 95% confidence level. Later, Kim and Naselsky (2010a) found that the Parity symmetry in the temperature map of WMAP 3 and 5 year data is anomalous at the level of 4 out of 1000 in the range $\delta\ell = [2, 18]$. This analysis have been repeated in the WMAP 7 year data confirming the anomaly at same level for a slightly wider range $\delta\ell = [2, 22]$ (Kim and Naselsky 2010b).

In this paper we address the issue of the parity asymmetry estimating the angular power spectra (APS) of the WMAP 7 year data at large angular scales by an optimal and unbiased estimator such as the quadratic maximum likelihood (QML) estimator. The same estimator is used to analyze 10000 simulated maps in which the noise is extracted from the low resolution noise covariance matrix of the WMAP 7 year data. This approach is novel since the estimates of the C_ℓ are made *jointly* in temperature and polarization allowing for a global, more robust estimate of all six CMB spectra. In particular, it allows to extend to polarization an analysis that has been performed only for temperature so far.

The used implementation of the QML is called *BolPol* and it has been already adopted in (Gruppuso et al. 2009) to compute the APS of the low resolution WMAP 5 year data and in (Paci et al. 2010) where the hemispherical power asymmetries have been studied for the same data set.

The paper is organized as follows. In Section 2 we describe the performed analysis, introducing the property of symmetry we expect the CMB maps to have in Subsection 2.1, providing the algebra of QML estimator in Subsection 2.2, specifying the used data set and the performed simulations in Subsection 2.3 and defining the suitable estimators in Subsection 2.4. Results are given in Section 3 and forecasts for Planck are provided in Section 4. Conclusions are drawn in Section 5.

2 DESCRIPTION OF THE ANALYSIS

2.1 Introduction

All-sky temperature maps, $T(\hat{n})$, are usually expanded in terms of Spherical Harmonics $Y_{\ell m}(\hat{n})$, with $\hat{n}$ being a direction in the sky, namely depending on the couple of angles (θ, ϕ):

$$a_{T,\ell m} = \int d\Omega\, Y^\star_{\ell m}(\hat{n})\, T(\hat{n})\,, \tag{1}$$

where $a_{T,\ell m}$ are the coefficients of the Spherical Harmonics expansion and $d\Omega = d\theta d\phi \sin\theta$. Under reflection (or Parity) symmetry ($\hat{n} \to -\hat{n}$), these coefficients behave as

$$a_{T,\ell m} \to (-1)^\ell\, a_{T,\ell m}\,. \tag{2}$$

Analogously for polarizations maps, taking into account the usual combination of Stokes parameters ($Q(\hat{n})$ and $U(\hat{n})$)

$$a_{\pm 2,\ell m} = \int d\Omega\, Y^\star_{\pm 2,\ell m}(\hat{n})\, (Q(\hat{n}) \pm iU(\hat{n}))\,, \tag{3}$$

where $Y_{\pm 2,\ell m}(\hat{n})$ are the Spherical Harmonics of spin 2 and $a_{\pm 2,\ell m}$ are the corresponding coefficients, it is possible to show that under Parity

$$a_{E,\ell m} \to (-1)^\ell\, a_{E,\ell m}, \tag{4}$$

$$a_{B,\ell m} \to (-1)^{\ell+1}\, a_{B,\ell m}\,, \tag{5}$$

where

$$a_{E,\ell m} = -(a_{2,\ell m} + a_{-2,\ell m})/2\,, \tag{6}$$

$$a_{B,\ell m} = -(a_{2,\ell m} - a_{-2,\ell m})/2i\,. \tag{7}$$

Eqs. (2), (4) and (5) show that the cross-correlations $C_\ell^{TB} = C_\ell^{EB} = 0$.

Further details can be found for example in (Zaldarriaga 1998), (Zaldarriaga and Seljak 1997) and explicit algebra is present in Appendix A.

2.2 Angular Power Spectra Estimation

In order to evaluate the APS we adopt the QML estimator, introduced in (Tegmark 1997) and extended to polarization in (Tegmark and de Oliveira-Costa 2001). In this section we describe the essence of such a method. Further details can be found in (Gruppuso et al. 2009).

Given a map in temperature and polarization $\mathbf{x} = (\mathbf{T}, \mathbf{Q}, \mathbf{U})$, the QML provides estimates $\hat{C}_\ell^X$ - with X being one of TT, EE, TE, BB, TB, EB - of the APS as:

$$\hat{C}_\ell^X = \sum_{\ell', X'} (F^{-1})_{\ell\ell'}^{XX'} \left[\mathbf{x}^t \mathbf{E}_{X'}^{\ell'} \mathbf{x} - tr(\mathbf{N}\mathbf{E}_{X'}^{\ell'})\right]\,, \tag{8}$$

where the $F_{XX'}^{\ell\ell'}$ is the Fisher matrix, defined as

$$F_{XX'}^{\ell\ell'} = \frac{1}{2} tr\left[\mathbf{C}^{-1} \frac{\partial \mathbf{C}}{\partial C_\ell^X} \mathbf{C}^{-1} \frac{\partial \mathbf{C}}{\partial C_{\ell'}^{X'}}\right]\,, \tag{9}$$

and the $\mathbf{E}_X^\ell$ matrix is given by

$$\mathbf{E}_X^\ell = \frac{1}{2} \mathbf{C}^{-1} \frac{\partial \mathbf{C}}{\partial C_\ell^X} \mathbf{C}^{-1}\,, \tag{10}$$

with $\mathbf{C} = \mathbf{S}(C_\ell^X) + \mathbf{N}$ being the global covariance matrix (signal plus noise contribution).

Although an initial assumption for a fiducial power spectrum C_ℓ^X is needed, the QML method provides unbiased estimates of the power spectrum contained in the map regardless of the initial guess,

$$\langle \hat{C}_\ell^X \rangle = \bar{C}_\ell^X\,, \tag{11}$$

where the average is taken over the ensemble of realizations (or, in a practical test, over Monte Carlo realizations extracted from $\bar{C}_\ell^X$). On the other hand, the covariance matrix associated to the estimates,

$$\langle \Delta\hat{C}_\ell^X \Delta\hat{C}_{\ell'}^{X'} \rangle = (F^{-1})_{\ell\ell'}^{XX'} , \quad (12)$$

does depend on the initial assumption for C_ℓ^X: the closer the guess to the true power spectrum is, the closer are the error bars to minimum variance. According to the Cramer-Rao inequality, which sets a limit to the accuracy of an estimator, Eq. (12) tells us that the QML has the smallest error bars. The QML is then an 'optimal' estimator.

2.3 Data set and Simulations

In this Section we describe the data set that we have considered. We use the temperature ILC map smoothed at 9.8 degrees and reconstructed at HealPix[1] (Gorski et al. 2005) resolution $N_{side} = 16$, the foreground cleaned low resolution maps and the noise covariance matrix in (Q, U) publicly available at the LAMBDA website [2] for the frequency channels Ka, Q and V as considered by Larson et al. (2010) for the low ℓ analysis. These frequency channels have been co-added as follows (Jarosik et al. 2007)

$$m_{tot} = C_{tot}(C_{Ka}^{-1} m_{Ka} + C_Q^{-1} m_Q + C_V^{-1} m_V) , \quad (13)$$

where m_i, C_i are the polarization maps and covariances (for i=Ka, Q and V) and

$$C_{tot}^{-1} = C_{Ka}^{-1} + C_Q^{-1} + C_V^{-1} . \quad (14)$$

This polarization data set has been extended to temperature considering the ILC map. We have added to the temperature map a random noise realization with variance of $1\mu K^2$ as suggested in Dunkley et al. (2009). Consistently, the noise covariance matrix for TT is taken to be diagonal with variance equal to $1\mu K^2$.

We have also performed a Monte-Carlo simulations in order to assess the significance of our results. A set of 10000 CMB + noise sky realizations has been generated: the signal extracted from the WMAP 7 years best fit model, the noise through a Cholesky decomposition of the noise covariance matrix. We have then computed the APS for each of the 10000 simulations by means of *BolPol* and build two figures of merit as explained in the next subsection.

Two masks are considered: one for T and one for Q and U. Monopole and dipole have been subtracted from the observed ILC map through the HealPix routine REMOVE-DIPOLE (Gorski et al. 2005).

2.4 Estimators

We define the following quantities

$$C_{+/-}^X \equiv \frac{1}{(\ell_{max} - 1)} \sum_{\ell=2,\ell_{max}}^{+/-} \frac{\ell(\ell+1)}{2\pi} \hat{C}_\ell^X \quad (15)$$

where $\hat{C}_\ell^X$ are the estimated APS obtained with *BolPol* for the power spectrum X = TT, TE, EE and BB. The sum is meant only over the even or odd ℓ (and this is represented respectively by the symbol + or −) with $\ell_{max} \geqslant 3$.

Therefore, two estimators can be built from Eq. (15) as follows: the ratio R^X, as performed in (Kim and Naselsky 2010a) or (Kim and Naselsky 2010b),

$$R^X = C_+^X / C_-^X , \quad (16)$$

and, in analogy to what performed for the hemispherical symmetry in (Paci et al. 2010), the difference D^X

$$D^X = C_+^X - C_-^X , \quad (17)$$

of the two aforementioned quantities. In the following, we drop the index X for R and D specifying every time we use them which is the spectrum they refer to.

For our application to WMAP data, both estimators have been considered for the TT spectrum but only the second one for the other spectra (EE, TE and BB). This is due the unfavorable signal-to-noise ratio of the WMAP data in polarization.

For X = TB and EB we simply use the average power

$$C^X \equiv \frac{1}{(\ell_{max} - 1)} \sum_{\ell=2,\ell_{max}} \frac{\ell(\ell+1)}{2\pi} \hat{C}_\ell^X . \quad (18)$$

3 RESULTS

APS for TT, TE and EE are given in Fig. 1 and for BB, TB and EB in Fig. 2. In these Figures we display both the *BolPol* estimates of the WMAP 7 year maps (black symbols) and the Monte-Carlo realizations from $\ell = 2$ to 32 (blue symbols). For TT and TE we display also the spectra provided by the WMAP team (red symbols) [3].

In Fig. 3 we show the estimator R and D for TT averaged in $2 \leqslant \ell \leqslant 22$ and in $2 \leqslant \ell \leqslant 33$. The probability to obtain a smaller value than the WMAP one is 0.47% for R in the range $\delta\ell = [2, 22]$ and 3.17% in the range $\delta\ell = [2, 33]$. For the D estimator the probability is 0.63% in the range $\delta\ell = [2, 22]$ and 3.17% in the range $\delta\ell = [2, 33]$. The upper left panel of Fig. 3 recovers the same level of anomaly claimed in Kim and Naselsky (2010b).

In Fig. 4 we plot the percentage related to the WMAP 7 year Parity anomaly for TT versus ℓ_{max} in the range $10 - 40$ for the two considered estimators. As evident there is not a single ℓ_{max} for which the TT anomaly shows up, but rather a characteristic scale, see also Kim and Naselsky (2010b). For the estimator of Eq. (16) the percentage anomaly is well below 1% for almost any choices of ℓ_{max} in the range $[15, 25]$ [4]. As also shown in Fig. 4 the estimator of Eq. (17) follows closely the other estimator although it is slightly less

[1] http://healpix.jpl.nasa.gov/
[2] http://lambda.gsfc.nasa.gov/

[3] Only these spectra are available on http://lambda.gsfc.nasa.gov/. Note that the WMAP TT estimates are obtained through a Maximum Likelihood code applied to the ILC map, whereas the WMAP TE estimates are obtained through a pseudo-C_ℓ method where the foreground cleaned V band is considered for Temperature and foreground cleaned Q and V bands are taken into account for Polarization.
[4] Only for $\ell_{max} = 21$ the estimator of Eq. (16) exhibits a percentage which is of the order of 1%.

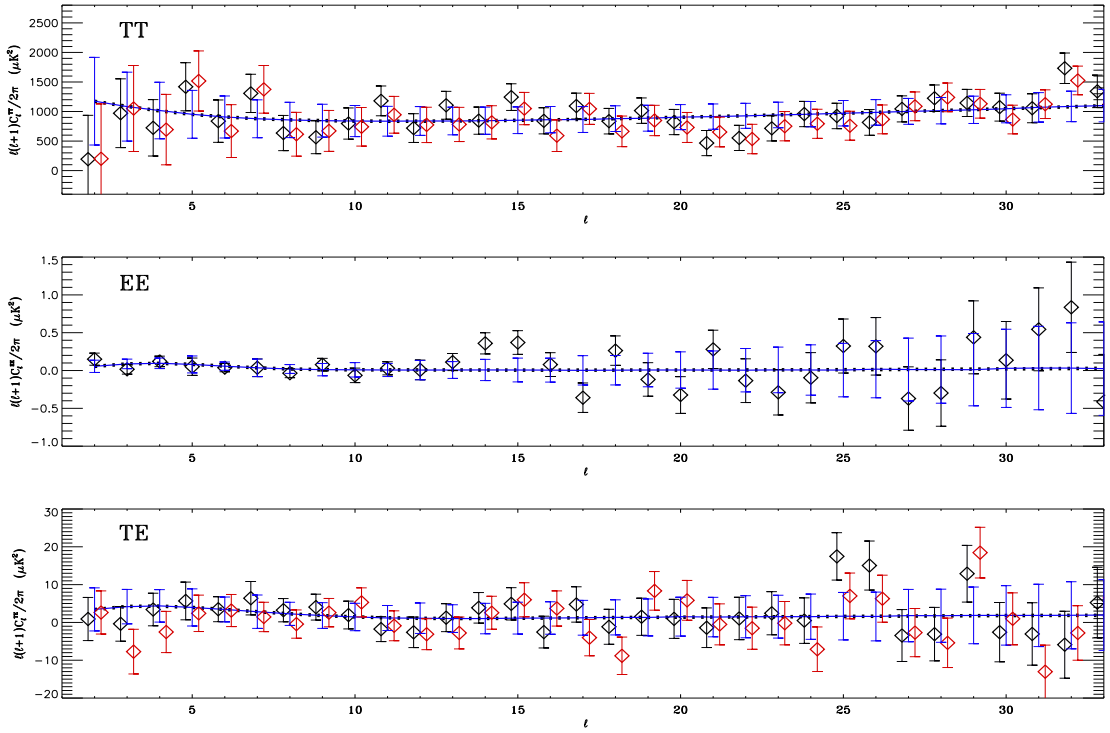

Figure 1. Estimates of TT (upper panel), EE (middle panel) and TE (lower panel) APS. Dotted lines stand for the Fiducial Power Spectrum, taken to be the best fit of the WMAP 7 year data. Blue lines with blue error bars represent the average and the standard deviation of a Monte Carlo made of 10000 sky realizations in which the full noise covariance is taken into account. Each realization has been analyzed with the *BolPol* code. Red symbols are for the WMAP 7 year estimates as provided at the following web site http://lambda.gsfc.nasa.gov/. Note that the WMAP TT estimates are obtained through a Maximum Likelihood code applied to the ILC map, whereas the WMAP TE estimates are obtained through a pseudo-C_ℓ method where the foreground cleaned V band is considered for Temperature and foreground cleaned Q and V bands are taken into account for Polarization. Black symbols are for the *BolPol* WMAP 7 year estimates where the black error bars are given through the Fisher matrix. Adopted resolution: $N_{side} = 16$.

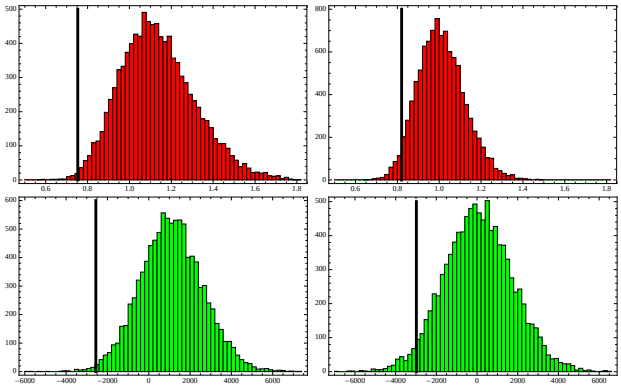

Figure 3. TT. Counts (y-axis) vs the estimator (x-axis). Upper histograms: Ratio for the range $\delta\ell = [2, 22]$ (left panel) and for the range $\delta\ell = [2, 33]$ (right panel). Lower histograms: Difference for the range $\delta\ell = [2, 22]$ (left panel) and for the range $\delta\ell = [2, 33]$ (right panel). Units for the estimator D are μK^2. The vertical line stands for the WMAP 7 year value.

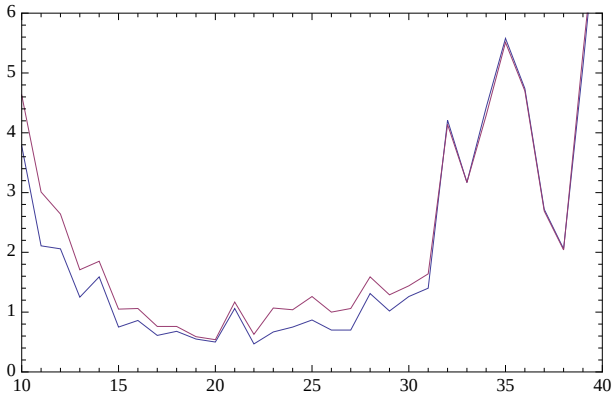

Figure 4. TT. Percentage of the WMAP 7 year value (y-axis) vs ℓ_{max} (x-axis). Blue line is for the ratio and the red line for the difference. This analysis shows that there is no single ℓ_{max} for which the TT anomaly shows up, but rather suggests the existence of a characteristic scale, see also Kim and Naselsky (2010b).

sensitive. Therefore, we find a whole multipole range, rather than a single ℓ_{max} value, where the WMAP 7 parity anomaly holds. This dims significantly the case for posterior biasing.

In Table 1 we provide the results for EE, TE and BB. As mentioned above, only D is considered and computed for the four following multipoles range $\delta\ell = [2, 4]$, $[2, 8]$, $[2, 16]$ and $[2, 22]$. No anomalies have been found and compatibility with Parity symmetry is obtained.

In Table 2 we provide the results for EB and TB where the estimator C is considered and computed for the same

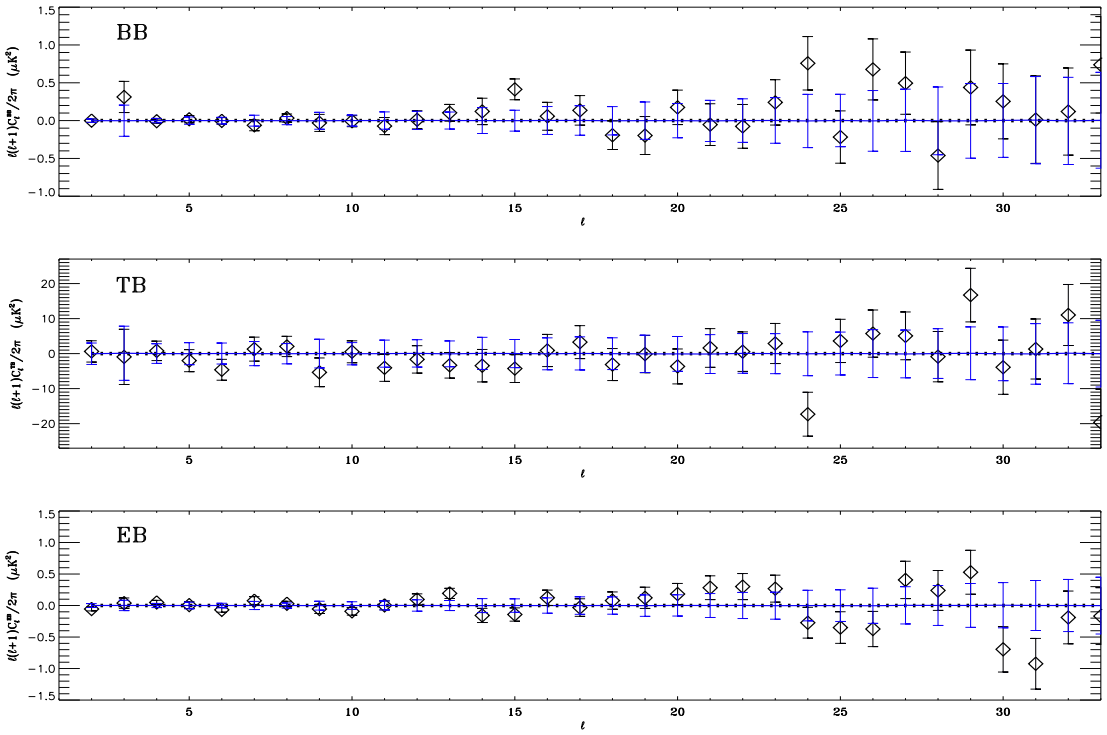

Figure 2. Estimates of BB (upper panel), TB (middle panel) and EB (lower panel) angular power spectrum. Conventions as in Figure 1.

Table 1. Probabilities (in percentage) to obtain a smaller value than the WMAP 7 year one

D	$\delta\ell = [2,4]$	$\delta\ell = [2,8]$	$\delta\ell = [2,16]$	$\delta\ell = [2,22]$
EE	93.09	76.21	44.27	46.61
TE	56.35	38.88	24.79	22.77
BB	7.97	13.42	11.70	44.31

Table 2. Probabilities (in percentage) to obtain a smaller value than the WMAP 7 year one

C	$\delta\ell = [2,4]$	$\delta\ell = [2,8]$	$\delta\ell = [2,16]$	$\delta\ell = [2,22]$
TB	51.78	39.42	6.71	10.55
EB	62.73	69.83	55.35	97.70

aforementioned four multipoles range. Both the spectra are well consistent with zero. Only the EB spectrum shows a mild anomaly in the range $\delta\ell = [2, 22]$ at the level of 97.7%. This is due to five estimates from $\ell = 18$ to $\ell = 22$ that are systematically larger than zero. When these points are excluded this mild anomaly drops. For example in the range $\delta\ell = [2, 16]$ the probability to obtain a smaller value than the WMAP one is 55.35%. The latter two estimators are shown in Fig. 5.

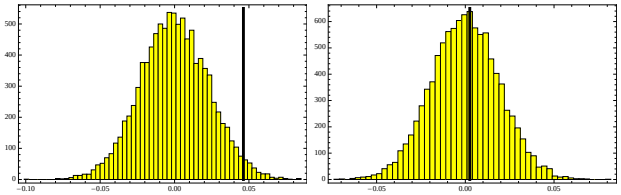

Figure 5. EB. Counts (y-axis) vs the estimator C (x-axis). Distribution of C for $\delta\ell = [2, 22]$ (left panel) and $\delta\ell = [2, 16]$ (right panel). Units are μK^2. The vertical line stands for the WMAP 7 year data.

3.1 Ka channel results

We have considered those WMAP products that are already foreground reduced (see subsection 2.3). However in order to test the case of a significant foreground contamination we have restricted our analysis to the Ka band since such a channel is expected to be more polluted by synchrotron and free-free emission than the others. Despite the lower signal-to-noise ratio our analysis for the Ka channel is fully consistent with that of the entire dataset: no anomaly is detected in polarization, while in temperature we do confirm its existence at the same level. These results, in our view, restrict (but of course not fully exclude) the chance for a significant foreground contamination. The lower signal-to-noise ratio shows up in an increase of the standard deviations associated to the probability distribution functions of the estimators. For example for the Ka band data set the standard deviation associated to the estimator D of EE in the ℓ range $[2, 22]$ grows 3.7 times with respect to the one obtained with the entire data set.

Table 3. Standard deviation for the D estimator computed in the range $\delta\ell = [2, 22]$. Units are μK^2.

σ_D	WMAP 7 year	Planck
TT	1517.17	1509.21
TE	20.19	9.08
EE	0.65	0.10
BB	0.69	0.04

Table 4. Standard deviation for the C estimator computed in the range $\delta\ell = [2, 22]$. Units are μK^2.

σ_C	WMAP 7 year	Planck
TB	0.95	0.19
EB	0.023	0.001

4 PLANCK FORECAST

In this Section we take into account the white noise level for 143 GHz channel of the Planck mission (Planck Collaboration 2005) launched into space on the 14th of May of 2009. As in Paci et al. (2010), we consider the nominal sensitivity of the Planck 143 GHz channel, taken as representative of the results which can be obtained after the foreground cleaning from various frequency channels. The 143 GHz channel has an angular resolution of $7.1'$ (FWHM) and an average sensitivity of $6\,\mu K$ ($11.4\,\mu K$) per pixel - a square whose side is the FWHM size of the beam - in temperature (polarization), after 2 full sky surveys. We assume uniform uncorrelated instrumental noise and we build the corresponding diagonal covariance matrix for temperature and polarization, from which, through Cholesky decomposition we are able to extract noise realizations. For this low noise level we apply the same procedure adopted for the Monte-Carlo simulations in Subsection 2.3. Thus, from the set of 10000 CMB + noise sky realizations, we find that:

- The T based estimators (both R and D) do not change much since at large scale the APS for T is dominated by cosmic variance and not by the noise.
- For EE, TE and BB it is possible to consider even the R estimator. See for example Fig. 6 where the R estimator is computed for EE in the range $\delta\ell = [2, 22]$ (left panel) and $\delta\ell = [2, 16]$ (right panel).
- The standard deviations for the D and C are evaluated in Table 3 and 4 for $\delta\ell = [2, 22]$ and compared to the WMAP 7 year ones.

5 DISCUSSIONS AND CONCLUSIONS

The Parity symmetry of the CMB pattern as seen by WMAP 7 year is tested *jointly in temperature and polarization* at large angular scale. We confirm the previously reported Parity anomaly for TT in the range $\delta\ell = [2, 22]$ at $> 99.5\%$ C.L. (Kim and Naselsky 2010b). Our resolution allows to extend the angular range up to $\ell = 40$ (see Fig. 4) finding a decrease of the anomaly for such a wider interval of multipoles. No violations have been found for EE, TE and BB which are tested here for the first time with a method analogous to the one employed for TT. The cross-spectra TB and EB are found to be well consistent with zero. The analysis has been performed through a Monte-Carlo made of 10000 sky maps in which the CMB maps are extracted from the WMAP 7 year fiducial model and the noise maps are obtained by Cholesky decomposition of WMAP 7 year noise covariance matrix for Ka, Q, V channels after foreground cleaning. WMAP 7 year maps and each of Monte-Carlo simulations have been analyzed with *BolPol* that is our F90 implementation of the QML method. As a byproduct the full APS of WMAP 7 year data is provided at large angular scale, see Figs. 1 and 2.

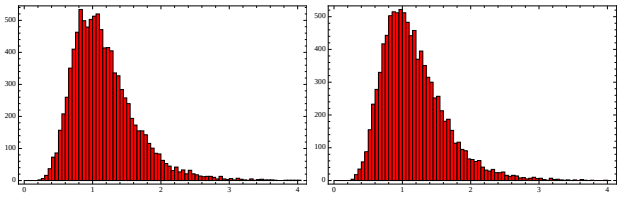

Figure 6. EE. Counts (y-axis) vs the estimator R (x-axis). Distribution of R for $\delta\ell = [2, 22]$ (left panel) and $\delta\ell = [2, 16]$ (right panel).

We have also forecasted Planck capabilities in probing Parity violations. Considering 10000 Monte-Carlo simulations we have evaluated the improvement with respect to WMAP 7 year sensitivity. These are shown in Table 3 and 4.

It is still unknown whether this anomaly [5] comes from fundamental physics or whether they are the residual of some unperfectly removed astrophysical foreground or systematic effect. As shown in Section 4, Planck data will allow one to build more precise estimators thanks to the high sensitivity of its instruments and the wide frequency coverage. Moreover Planck is observing the sky with a totally different scanning strategy with respect to WMAP, which is a benefit from the point of view of systematic effects analysis. Thus Planck data are awaited with great interest in order to confirm or discard these anomalies, making real the possibility to have more stringent constraints on the ΛCDM model.

ACKNOWLEDGEMENTS

We acknowledge the use of the BCX and SP6 at CINECA under the agreement INAF/CINECA and the use of computing facility at NERSC. We acknowledge use of the HEALPix (Gorski et al. 2005) software and analysis package for deriving the results in this paper. We acknowledge the use of the Legacy Archive for Microwave Background Data Analysis (LAMBDA). Support for LAMBDA is provided by the NASA Office of Space Science. Work supported by ASI through ASI/INAF Agreement I/072/09/0 for the Planck LFI Activity of Phase E2.

[5] Of course similar arguments apply to the other anomalies as well.

APPENDIX A: PARITY SYMMETRY

In this appendix we explicitly show the Eqs. (2), (4) and (5).

A1 Temperature

In analogy to the definition given in Eq. (1) we write

$$a^{(P)}_{T,\ell m} = \int d\Omega\, Y^\star_{\ell m}(\hat{n})\, T^{(P)}(\hat{n})\,, \tag{A1}$$

where $T^{(P)}(\hat{n}) = P[T(\hat{n})]$ with P being the parity operator. By definition $P[T(\hat{n})] = T(-\hat{n})$, i.e. under reflection symmetry $\hat{n} \to -\hat{n}$ [6] that in polar coordinates is equivalent to

$$\theta \;\to\; \pi - \theta\,, \tag{A2}$$

$$\phi \;\to\; \phi + \pi\,. \tag{A3}$$

Hence Eq. (A1) can be rewritten as

$$a^{(P)}_{T,\ell m} = \int d\Omega\, Y^\star_{\ell m}(-\hat{n})\, T(\hat{n})\,, \tag{A4}$$

where the integration variables have been changed following Eqs. (A2),(A3) in order to absorb the minus in the argument of T [7]. The Spherical Harmonics $Y_{\ell m}$ are related to Legendre functions P^m_ℓ as

$$Y_{\ell m}(\theta,\phi) = \sqrt{\frac{2\,\ell+1}{4\pi}\frac{(\ell-m)!}{(\ell+m)!}} P^m_\ell(\cos\theta)\, e^{im\phi}\,, \tag{A5}$$

therefore

$$Y_{\ell m}(\pi-\theta,\phi+\pi) = (-1)^m (-1)^{\ell+m} Y_{\ell m}(\theta,\phi)\,, \tag{A6}$$

where it has been used that

$$P^m_\ell(\cos(\pi-\theta)) = (-1)^{(\ell+m)} P^m_\ell(\cos(\theta))\,. \tag{A7}$$

Replacing Eq. (A6) in Eq. (A4) gives

$$a^{(P)}_{T,\ell m} = (-1)^\ell \int d\Omega\, Y^\star_{\ell m}(\hat{n})\, T(\hat{n}) = (-1)^\ell\, a_{T,\ell m}\,, \tag{A8}$$

that shows Eq. (2).

A2 Polarization

Let start considering the E mode. By definition

$$a^{(P)}_{E,\ell m} = -\frac{1}{2}\left(a^{(P)}_{2,\ell m} + a^{(P)}_{-2,\ell m}\right)\,, \tag{A9}$$

where

$$a^{(P)}_{\pm 2,\ell m} = \int d\Omega\, Y^\star_{\pm 2,\ell m}(\hat{n})\, [Q \pm iU]^{(P)}(\hat{n})\,. \tag{A10}$$

Since $Q \pm iU$ is isomorphic to a bi-dimensional vector (see footnote 4) than

$$[Q \pm iU]^{(P)}(\hat{n}) \;=\; Q^{(P)}(\hat{n}) \mp iU^{(P)}(\hat{n}) \tag{A11}$$

$$\;=\; Q(-\hat{n}) \mp iU(-\hat{n})\,. \tag{A12}$$

Replacing Eqs. (A12) and (A10) in Eq. (A9) we find

$$a^{(P)}_{E,\ell m} = -\int d\Omega\left[X^\star_{1,\ell m}(-\hat{n})\, Q(\hat{n}) - X^\star_{2,\ell m}(-\hat{n}) iU(\hat{n})\right] \tag{A13}$$

where we have changed the integration variables considering Eqs. (A2),(A3) and where we have used the conventions of (Zaldarriaga 1998) defining $X_{1/2,\ell m}$ as

$$X_{1,\ell m}(\theta,\phi) = -\frac{1}{2}\left(Y_{2,\ell m}(\theta,\phi) + Y_{-2,\ell m}(\theta,\phi)\right)\,, \tag{A14}$$

$$X_{2,\ell m}(\theta,\phi) = -\frac{1}{2}\left(Y_{2,\ell m}(\theta,\phi) - Y_{-2,\ell m}(\theta,\phi)\right)\,. \tag{A15}$$

Since in (Zaldarriaga 1998) $X_{1/2,\ell m}$ are expressed in terms of Legendre polyniomials it is easy to show that

$$X_{1,\ell m}(\pi-\theta,\phi+\pi) = (-1)^\ell X_{1,\ell m}(\theta,\phi)\,, \tag{A16}$$

and

$$X_{2,\ell m}(\pi-\theta,\phi+\pi) = (-1)^{\ell+1} X_{2,\ell m}(\theta,\phi)\,. \tag{A17}$$

Replacing Eqs. (A16),(A17) back into Eq. (A13) and using again Eqs. (A14),(A15) we find Eq. (4)

$$a^{(P)}_{E,\ell m} = (-1)^\ell a_{E,\ell m}\,. \tag{A18}$$

Repeating the same steps but starting from

$$a^{(P)}_{B,\ell m} = -\frac{1}{2i}\left(a^{(P)}_{2,\ell m} - a^{(P)}_{-2,\ell m}\right)\,, \tag{A19}$$

one finds Eq. (5), i.e.

$$a^{(P)}_{B,\ell m} = (-1)^{\ell+1} a_{B,\ell m}\,. \tag{A20}$$

[6] This holds in 3 dimensions. Note that a Parity transformation in two dimensions is $(x,y) \to (x,-y)$ or $(x,y) \to (-x,y)$. In other words the transformation $(x,y) \to (-x,-y)$ is not a parity transformation since is equivalent to a rotation.

[7] $\int d\Omega$ is invariant under Parity transformation. This is trivial to show in cartesian coordinates.

REFERENCES

Abramo L. R., Bernui A., Ferreira I. S., Villela T. and Wuensche C. A., Phys. Rev. D **74**, 063506 (2006) [arXiv:astro-ph/0604346].

Bennett C. L. *et al.*, arXiv:1001.4758 [astro-ph.CO].

Bernui A. and Reboucas M. J., Phys. Rev. D **81**, 063533 (2010) [arXiv:0912.0269 [astro-ph.CO]].

Bernui A., Reboucas M. J. and Teixeira A. F. F., arXiv:1005.0883 [astro-ph.CO].

Copi C. J., Huterer D. and Starkman G. D., Phys. Rev. D **70**, 043515 (2004) [arXiv:astro-ph/0310511].

Copi C. J., Huterer D., Schwarz D. J. and Starkman G. D., Phys. Rev. D **75**, 023507 (2007) [arXiv:astro-ph/0605135].

Copi C. J., Huterer D., Schwarz D. J. and Starkman G. D., Mon. Not. Roy. Astron. Soc. **399**, 295 (2009) [arXiv:0808.3767 [astro-ph]].

Copi C. J., Huterer D., Schwarz D. J. and Starkman G. D., arXiv:1004.5602 [astro-ph.CO].

Cruz M., Martinez-Gonzalez E., Vielva P. and Cayon L., Mon. Not. Roy. Astron. Soc. **356**, 29 (2005) [arXiv:astro-ph/0405341].

Cruz M., Martinez-Gonzalez E. and Vielva P., arXiv:0901.1986 [astro-ph].

Dunkley J. et al. (WMAP), apj SS 180 (2009) 306, arXiv:0803.0586 [astro-ph].

Eriksen H. K., Hansen F. K., Banday A. J., Gorski K. M. and Lilje P. B., Astrophys. J. **605** (2004) 14 [Erratum-ibid. **609** (2004) 1198] [arXiv:astro-ph/0307507].

Eriksen H. K., Banday A. J., Gorski K. M., Hansen F. K. and Lilje P. B., Astrophys. J. **660**, L81 (2007) [arXiv:astro-ph/0701089].

Gorski K.M., Hivon E., Banday A.J., Wandelt B.D., Hansen F.K., Reinecke M. and Bartelmann M., 2005, HEALPix: A Framework for High-resolution Discretization and Fast Analysis of Data Distributed on the Sphere, Ap.J., 622, 759-771

Gruppuso A., de Rosa A., Cabella P., Paci F., Finelli F., Natoli P., de Gasperis G. and Mandolesi N. Mon. Not. Roy. Astron. Soc. **400**, 1, (2009) arXiv:0904.0789 [astro-ph.CO].

Gruppuso A. and Burigana C., JCAP **0908**, 004 (2009) [arXiv:0907.1949 [astro-ph.CO]].

Gruppuso A. and Gorski K. M., JCAP **1003**, 019 (2010) [arXiv:1002.3928 [astro-ph.CO]].

Hansen F. K., Banday A. J. and Gorski K. M., Mon. Not. Roy. Astron. Soc. **354**, 641 (2004) [arXiv:astro-ph/0404206].

Hansen F. K., Banday A. J., Gorski K. M., Eriksen H. K. and Lilje P. B., Astrophys. J. **704**, 1448 (2009) [arXiv:0812.3795 [astro-ph]].

Hoftuft J., Eriksen H. K., Banday A. J., Gorski K. M., Hansen F. K. and Lilje P. B., Astrophys. J. **699**, 985 (2009) [arXiv:0903.1229 [astro-ph.CO]].

Jarosik N. *et al.* [WMAP Collaboration], Astrophys. J. Suppl. **170**, 263 (2007) [arXiv:astro-ph/0603452].

Kim J. and Naselsky P., Astrophys. J. **714**, L265 (2010a) [arXiv:1001.4613 [astro-ph.CO]].

Kim J. and Naselsky P., (2010b) arXiv:1002.0148 [astro-ph.CO].

Komatsu E. *et al.*, arXiv:1001.4538 [astro-ph.CO].

Land K. and Magueijo J., Phys. Rev. Lett. **95**, 071301 (2005a) [arXiv:astro-ph/0502237].

Land K. and Magueijo J., Phys. Rev. D **72**, 101302 (2005) [arXiv:astro-ph/0507289].

Larson D. *et al.*, arXiv:1001.4635 [astro-ph.CO].

Paci F., Gruppuso A., Finelli F., Cabella C., De Rosa A., Mandolesi N. and Natoli P., in press on Mon. Not. Roy. Astron. Soc. (2010) arXiv:1002.4745 [astro-ph.CO].

Pietrobon D., Cabella P., Balbi A., Crittenden R., de Gasperis G. and Vittorio N., Mon. Not. Roy. Astron. Soc. Letters (2009), **402**, Issue 1, pp. L34-L38 arXiv:0905.3702 [astro-ph.CO].

Planck Collaboration, ESA publication ESA-SCI (2005)/1 arXiv:astro-ph/0604069.

Schwarz D. J., Starkman G. D., Huterer D. and Copi C. J., Phys. Rev. Lett. **93**, 221301 (2004) [arXiv:astro-ph/0403353].

Tegmark M., Phys. Rev. D **55**, 5895 (1997)

Tegmark M. and de Oliveira-Costa A., Phys. Rev. D **64** (2001) 063001

Tegmark M., de Oliveira-Costa A. and Hamilton A., Phys. Rev. D **68**, 123523 (2003) [arXiv:astro-ph/0302496].

Vielva P., Martinez-Gonzalez E., Barreiro R. B., Sanz J. L. and Cayon L., Astrophys. J. **609**, 22 (2004) [arXiv:astro-ph/0310273].

Vielva, P., Wiaux, Y., Martínez-González, E., & Vandergheynst, P. 2007, MNRAS, 381, 932

Weeks J. R., arXiv:astro-ph/0412231.

Wiaux Y., Vielva P., Martinez-Gonzalez E. and Vandergheynst P., Phys. Rev. Lett. **96**, 151303 (2006) [arXiv:astro-ph/0603367].

Zaldarriaga M., Astrophys. J. **503**, 1 (1998) [arXiv:astro-ph/9709271].

Zaldarriaga M. and Seljak U., Phys. Rev. D **55**, 1830 (1997) [arXiv:astro-ph/9609170].